Available online at www.sciencedirect.com

SciVerse ScienceDirect

Ceramics International 39 (2013) 7379–7386

CERAMICS INTERNATIONAL

www.elsevier.com/locate/ceramint

Porous $ZnAl_2O_4$ spinel nanorods: High sensitivity humidity sensors

Baochang Cheng*, Zhiyong Ouyang, Baixiang Tian, Yanhe Xiao, Shujin Lei

Institute for Advanced Studying and School of Materials Science and Engineering, Nanchang University, Jiangxi 330031, PR China

Received 29 January 2013; received in revised form 22 February 2013; accepted 23 February 2013
Available online 1 March 2013

Abstract

Porous zinc aluminate ($ZnAl_2O_4$) spinel nanorods were synthesized via a homogeneous co-precipitation approach followed by a heat treatment at 900 °C. The porous rod-like nanostructures not only increase the efficiency of adsorption sites, but also promote the dissociation of water adsorbed on nanorod boundaries and pore-walls. Moreover, they also provide an effective and fast channel for the transport of water vapor and liquid. Therefore, the impedance signal of the sensors based on the porous nanorods presents high sensitivity, good linearity, small hysteresis, and fast response/recovery time to humidity. Additionally, the sensors are also relatively stable to humidity for a long time. This study demonstrates that porous $ZnAl_2O_4$ nanorods are a promising platform for the construction of humidity sensors.

Keywords: B. Porosity; D. Spinels; E. Sensor; Nanostructures

1. Introduction

Humidity is a physical parameter denoting the degree of dryness in the atmosphere, and it is a crucial factor in food processing, textile technology, places such as storage areas, computer rooms, hospitals, museums and so on. Therefore, it is necessary to design well-performed humidity sensors, which usually exhibit the characters of high sensitivity, best linearity, good reliability and stability, rapid response and recovery, and small hysteresis [1]. In recent years, researchers have developed humidity sensors using changes in capacitance, frequency, refractive index, and impedance as sensing mechanisms [2–4]. These properties are determined by the sensing medium material, porosity, surface area, and pore size distribution. At present, many kinds of materials including electrolyte [5], organic polymer [6] and ceramic materials [7] have been produced as humidity sensor bodies. Among them, ceramic materials have been widely studied due to their unique properties such as the relatively high thermal, chemical and mechanical stability [8,9]. Metal oxide ceramic TiO_2 [10], ZnO [11], ferrite [7], Al_2O_3 [12,13], and $(Ba,Sr)TiO_3$ [14,15] have been extensively used as humidity sensors for their excellent water adsorbing/removing property. In particular, they can remain stable at elevated temperatures and high humidity and have high sensitivity for porous ceramic based capacitive sensors. Moreover, they have nonlinear characteristics with hysteresis and require only temporary heating. Because of the water molecule chemisorption, however, ceramic-based humidity sensors still lack sufficient sensitivity over wide humidity ranges and reversibility, and drift in base resistance with time, which restrains the development of humidity sensors in applications. With a large surface to volume ratio and the effective electron transport, one-dimensional (1D) nanostructures have been regarded as the ideal candidates for translating the chemical species (gas and moisture) recognition into an electrical signal [16]. Up to now, many sensitive chemical sensors have been obtained based on the 1D nanostructures [17–21].

$ZnAl_2O_4$ is a typical ceramic material. Our previous work has shown that porous rod-like $ZnAl_2O_4$ nanostructures, possessing a large specific surface area of 93.2 m^2/g and a relatively narrow size distribution in the range of 6–20 nm, can be fabricated readily through an annealing transform of layered composite precursors at 900 °C [22]. Due to capillary condensation effects, furthermore, the hysteresis loop can be observed in a relatively high pressure

*Corresponding author. Tel.: +86 13576906262; fax: +86 791 83969329.
E-mail address: bcheng@vip.sina.com (B. Cheng).

0272-8842/$ - see front matter © 2013 Elsevier Ltd and Techna Group S.r.l. All rights reserved.
http://dx.doi.org/10.1016/j.ceramint.2013.02.077

range of 0.7–0.98P_0 by the nitrogen adsorption/desorption isotherms [22]. The immense surface-to-volume ratio can increase the adsorption sites for water vapor efficiently so that the sensitivity of the porous-nanostructures-based sensor may be enhanced. For the abundant void fraction, it can provide an effective channel for vapor transport. In particular, the flow rate of liquid can be enhanced significantly in tube-like nanostructures [14], indicating the response and recovery speed of the porous-nanostructures-based sensor to humidity is much faster. The air in the pores is replaced by adsorbed water as the ambient humidity level increases, and the permittivity can show a huge increase since the dielectric constant of water ($\varepsilon_w \approx 80$) is much higher than that of air (≈ 1) at room temperature, which can considerably amplify the capacitance response at a low relative humidity (RH) content [23]. Recent studies also show that a highly reproducible, wide-range humidity sensor can be achieved using the nanodimensional pores with a narrow size distribution [24,25]. On the basis of these advantageous performances, therefore, porous $ZnAl_2O_4$ nanorods are suitable for sensing application, where the very high sensitivities and responsiveness should be expected. In this work, the sensor based on porous $ZnAl_2O_4$ nanorods is reported, and its humidity properties are investigated in detail.

2. Material and methods

2.1. Synthesis and characterization of materials

Firstly, the composite precursors were synthesized by means of a homogeneous co-precipitation method with the assistance of a surfactant. Detailed description of the method can be found in our previous publication [22]. $Zn(NO_3)_3 \cdot 6H_2O$, $Al(NO_3)_3 \cdot 9H_2O$, hexadecyltrimethylammonium bromide [$(C_{16}H_{33})N^+(CH_3)_3 \cdot Br^-$, CTAB], urea [$CO(NH_2)_2$], and deionized water were mixed at a molar ratio of 1:2:1:5:400 and stirred to obtain a transparent solution. Then, the solution was put into a Teflon-lined stainless steel autoclave and kept at a reaction temperature of 125 °C for 15 h. The obtained white slurry was collected, washed, and dried. After that the resulting powder was annealed at 900 °C for 3 h in an air atmosphere to obtain a pure $ZnAl_2O_4$ crystallographic structure.

The structure and morphology of the samples were characterized using x-ray diffraction (XRD, Bruker D-8 with Cu-Kα radiation), field emission environmental scanning electron microscopy (FE-ESEM, FEI Quanta 200F), and high-resolution transmission electron microscopy (HRTEM; JEOL JEM-2010, at 200 kV).

2.2. Fabrication and measurement of humidity sensor based on porous $ZnAl_2O_4$ nanorods

Firstly, the post-annealed $ZnAl_2O_4$ powder was pressed into a pellet under 10 MPa with a thickness of about 0.4 cm and a diameter of 1.5 cm. Then, Ag electrodes were screen printed on both sides of the pellet, and Cu wire was connected to Ag electrode as lead wire. Finally, the humidity sensor was fabricated after aging at 95% RH with a voltage of 1 V, 100 Hz for 24 h. The characteristic curves of humidity sensitivity were measured on a precision LCR meter (Agilent-4284A). The measured frequency was in the range from 40 Hz to 1 MHz, and the measured voltage was 1 V. The controlled humidity environments were achieved using supersaturation aqueous solutions of different salts of LiCl, $MgCl_2$, $Mg(NO_3)_2$, KCl, and KNO_3 in a closed glass vessel at an ambient temperature of 25 °C, which yielded approximately 11%, 33%, 54%, 85% and 95% RH levels, respectively [26].

3. Results and discussion

3.1. Structure characteristics

The representative XRD patterns of the samples synthesized at 125 °C in aqueous solution and post-calcined at 900 °C are both shown in Fig. 1. As evident from the XRD analysis, the samples obtained from the aqueous solution are mainly composed of an end-centered $NH_4Al(OH)_2CO_3$ (JCPDS no. 76-192376–1923). In addition, some very weak diffraction peaks of rhomb-centered hexagonal $Zn_6Al_2(OH)_{16}CO_3 \cdot nH_2O$ (JCPDS no. 38-048638–0486) and $Zn_4Al_2(OH)_{12}CO_3 \cdot nH_2O$ (JCPDS no. 48-102348–1023) are also observed. After the precipitate precursor is post-annealed at 900 °C for 3 h, all reflections in the XRD pattern can be indexed well to a pure face-centered cubic $ZnAl_2O_4$ with a spinel structure, close to the reported values (JCPDS no. 74-113874–1138). Although the diffraction intensity of the $Zn_6Al_2(OH)_{16}CO_3 \cdot nH_2O$ and $Zn_4Al_2(OH)_{12}CO_3 \cdot nH_2O$ phase is very weak in contrast with $NH_4Al(OH)_2CO_3$ on the basis of XRD measurement, the product post-annealed at 900 °C completely consists of $ZnAl_2O_4$, indicating that Zn^{2+} ions occupy substitutionally the sites of cations and are embedded in the middle of the inter-layers of layered $NH_4Al(OH)_2CO_3$ structures [27].

The FE-ESEM image provides the general morphology of the products post-calcined at 900 °C, as shown in Fig. 2a. From the image, it can be seen that the sample is composed of relatively uniform 1D nanostructures with

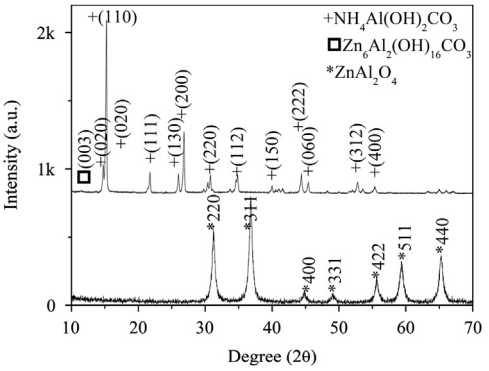

Fig. 1. XRD patterns of the products: (a) synthesized for 15 h in aqueous solution and (b) post-annealed at 900 °C for 3 h.

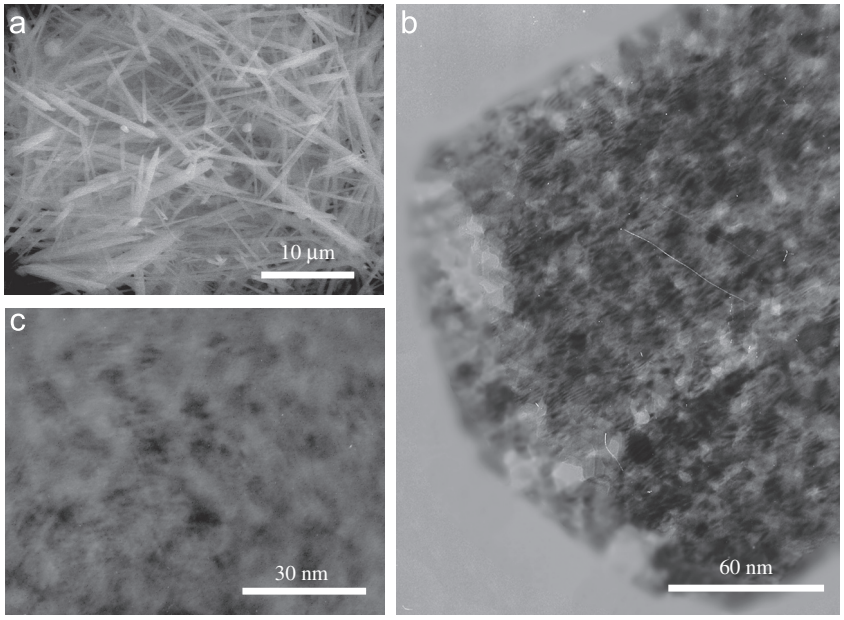

Fig. 2. FE-ESEM (a), and TEM (b) and (c) images of the sample post-annealed at 900 °C for 3 h.

diameters of about 100–200 nm and lengths ranging from several to tens of micrometers. Moreover, the nanorods remain free-standing, remarkably with no sign of aggregation through the whole heat treatment process. As can be seen from TEM images shown in Fig. 2b and c, a large quantity of irregular pores exist in the nanorod, indicating the formation of porous rod-like nanostructures.

3.2. Humidity sensing characteristics

To determine the humidity sensitivity of the sensor and evaluate the sensor's behavior to humidity changes based on the porous $ZnAl_2O_4$ nanorods, its impedance at different frequencies as a function of RH was measured. The sensor's sensitivity is defined as the slope of the curve of sensor response (impedance in this case) vs. humidity concentration, and the magnitude of the impedance mainly reflects the conductance of the sensing materials. Although the impedance as a function of RH presents a nonlinear tendency with increasing RH, the impedance follows a logarithmic increase with increasing RH and exhibits good linear log(Impedance) toward RH in the range of 11–95%. Linear plots of the log(Impedance) as a function of relative humidity (11–95% RH) for different frequencies are shown in Fig. 3. As seen from the humidity plots, the sensor's impedance decreases with increasing the RH at all measuring frequencies, especially in low frequency, e.g. at 40 Hz, and it changes from 7×10^3 to 70 kΩ as RH varies from 11% to 95%, implying a relatively high sensitivity. Additionally, the slope of linear fit curves decreases from −0.02309 to −0.00619 with the increase of measurement frequency from 40 Hz to 1 MHz, indicating a decrease in sensitivity. The relatively high sensitivity demonstrates that porous rod-like nanostructures can enlarge efficient

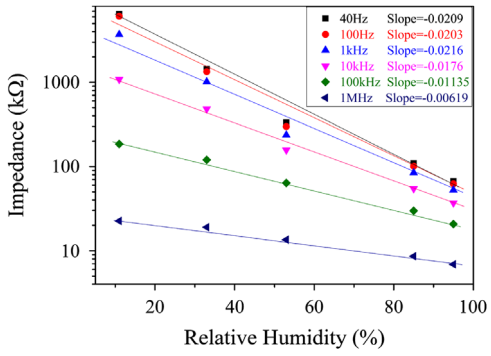

Fig. 3. Dependence of impedance on RH for the sensor based on porous $ZnAl_2O_4$ nanorods measured at various frequencies.

adsorption sites for water vapor and promote the dissociation of adsorbed water on the nanorod boundaries and pore-walls, which contributes to the increase of the surface electrical conductivity and results in a large decrease in impedance with increasing RH. Therefore, the sensor based on the porous $ZnAl_2O_4$ nanorods can show a relatively high sensitivity and a wide range of humidity detection. In high frequency ranges, the impedance plots become flat, indicating that adsorbed water cannot be polarized at higher frequencies [28].

Since the capacitance property of the sensor vs. RH can reflect the dielectric coefficient of the sensing materials, i.e. the polarization property, it was also measured in different frequency ranges, as shown in Fig. 4. It can be seen that the capacitance not only strongly depends on the measured frequencies, but also on the RH levels. At the frequency lower than 100 Hz, a relatively large variation can be achieved, for instance, the capacitance can change from about 1000 to 30,000 pF as RH goes to 95% from 11%

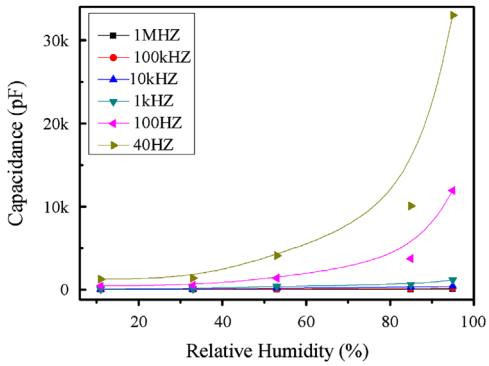

Fig. 4. Capacitance vs. RH of the humidity sensor measured at different frequencies.

at 40 Hz. When the frequency is higher than 10 kHz, however, the change of capacitance is inconspicuous. The higher the measurement frequency is, the smaller the capacitance change is. From the capacitance–RH curve given in Fig. 4, it was also observed that the capacitance shows a relatively slow increase in the low RH range of 11–85%, and a sharp rise can be detected however, as RH reaches a certain range (above about 85%), especially at low measurement frequencies.

In low frequency ranges, the electrical field direction changes slowly so that the orientation polarization of adsorbed water appears noticeably. Due to different relative dielectric constants between water vapor (140 °C, 1.00785) and liquid (close to 80), the higher the RH is, the more the water vapor is adsorbed and condensed, and thus the stronger the polarization is. As a consequence, the dielectric constant (capacitance) increases with RH. However, in high frequency ranges, the electrical field direction changes fast so that the polarization of the water cannot catch up with it, and therefore, the dielectric constant is small and independent of RH [28,29].

It is well known that physisorption includes pore-wall adsorption and capillary condensation. Condensation occurs in all the pores with radius up to r given by the Kelvin equation (contact angle = 0) [30].

$$r = \frac{\gamma v}{RT \ln(1/RH)},$$

where γ, v, T, and R stand for the surface tension, molar volume, absolute temperature, and gas constant, respectively. At relatively low RH levels, very thin layers of water molecules are formed on the nanorod boundaries and pore-walls. Subsequently, multilayer adsorption happens as the humidity level increases. Because the dielectric constant of water ($\varepsilon_w \approx 80$) is much higher than that of air (≈ 1) at room temperature, the capacitance slowly increases with humidity up to 85% RH. When RH exceeds 85%, however, Kelvin radius increases dramatically with RH [31]. Thus, capillary condensation effects become predominant gradually, and wider and wider pores will be filled by water vapor. In addition, water vapor can also fill into the electrode/nanorod film interface. As a consequence, the capacitance (dielectric constant) can increase sharply. This demonstrates that a humidity level around 85% might be the critical transition humidity for the porous $ZnAl_2O_4$ nanorod-based sensor, under which the interaction mechanism between water vapor and porous nanorods changes from the multilayer physisorption adsorption to the capillary condensation.

The relatively large humidity hysteresis has been a serious problem in the practical humidity sensors. The adsorption/desorption hysteresis for the $ZnAl_2O_4$ nanorod-based sensor was also characterized in our experiment through measuring the impedance dependent on cyclic humidity change at a frequency of 100 Hz, and the result is shown in Fig. 5. The black line measured from low to high RH represents the adsorption process, and the red line measured in the opposite direction represents the desorption process. The isotherms can be described as type IV, and a maximum humidity hysteresis of about 2% is observed under 70% RH. This relatively small hysteresis is essentially negligible and indicates a good reliability of the sensor.

At higher RH levels, the appearance of the largest hysteresis indicates that it distinctly contributes from the capillary condensation [32]. Since Kelvin radius increases dramatically with increasing RH, wider and wider pores will be filled, and the pores will get empty as it decreases. Generally, there are two different contact angles on the two branches of the loop. One is an advancing contact angle (θ_a) as the pores are filling, whereas the other is a "receding" contact angle (θ_r) as they are emptying. Since θ_a is greater than θ_r, according to the Kelvin equation, for a given value of pore size, the value of pressure during the desorption is less than that during the adsorption causing the hysteresis [33]. The relatively small hysteresis indicates that the difference between advancing and receding contact angles might be very small.

To determine the response/recovery speed of the sensor based on the porous $ZnAl_2O_4$ nanorods, the characteristic curve of water molecule adsorption and desorption process for one cycle was also measured as shown in Fig. 6. When the sensor was exposed to a moist air of 95% RH from a relatively dry air of 11% RH, the impedance of the sensor

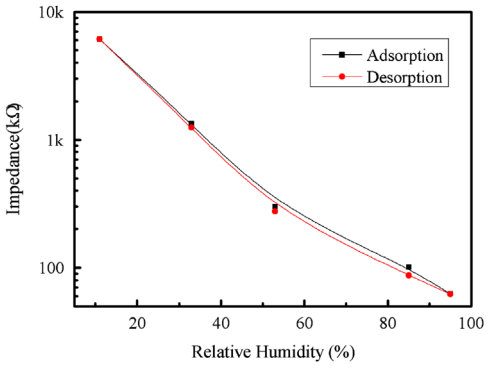

Fig. 5. Humidity hysteresis characteristic of the humidity sensor measured at 100 Hz. (For interpretation of the references to color in this figure, the reader is referred to the web version of this article.)

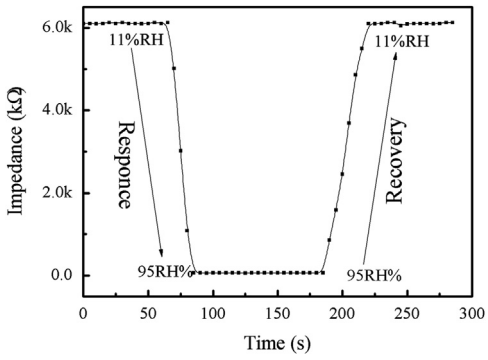

Fig. 6. Response and recovery characteristic of the humidity sensor measured at 100 Hz.

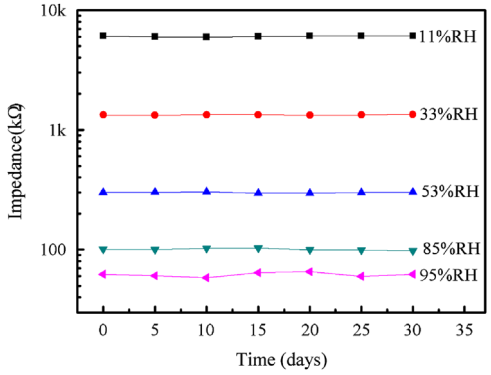

Fig. 7. Impedance stability of the porous $ZnAl_2O_4$ nanorod-based sensor measured at 100 Hz.

rapidly decreased and then gradually reached a relatively stable value. Subsequently, when the sensor was switched to the dry air of 11% RH again, the impedance abruptly increased, and rapidly reached a relatively stable value. The response and recovery time, defined as the time required to reach 90% of the final equilibrium value, was around 15 and 30 s respectively. In addition, it also showed a good reproducibility. These results indicate that the interaction between water vapor and $ZnAl_2O_4$ porous nanorods should be mainly dominated by physisorption, while chemisorption plays a minor role. Moreover, the transport of water vapor and liquid should be very fast in the nanopores so that the sensor can be practically used.

The long-term stability of gas sensors is also one of the most important characteristics, especially in a humid environment. To test the stability, the sensor was exposed in air for 30 days, followed by measuring impedances at various RH levels every 5 days. As shown in Fig. 7, the impedances show nearly no change at each humidity region for 5 days, which directly confirms that the impedance of the sensor is relatively stable to the exposure to the water in the air.

3.3. Discussion on sensing principles

In order to study the transport behavior in an A.C. field and find out the working principle of the humidity sensor based on porous $ZnAl_2O_4$ nanorods, the impedance spectra for different RH levels within the frequency range from 40 Hz to 1 MHz were taken. The total impedance was resolved into real (Z_{re}) and imaginary (Z_{im}) parts, and then complex impedance plots (Nyquist plots) were constructed, as shown in Figs. 8 and 9. From Fig. 8, it can be seen that at a relatively low RH of 11% an approximately inclined semicircle is observed in the Z_{im} vs. Z_{re} curve. When the RH increases to about 33%, however, two depressed semicircles can be observed obviously in the complex impedance plots. Furthermore, their sizes both decrease with the increasing RH. It is worth noting that the second is smaller than the first as RH varies in the range of 33–85%, whereas they become very close at RH higher

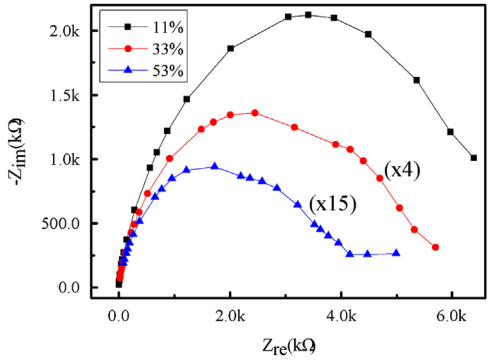

Fig. 8. Complex impedance plots of the humidity sensor based on $ZnAl_2O_4$ nanorods measured in the relatively low RH values of 11%, 33% and 53% within the frequency range from 40 Hz to 1 MHz.

than 85%. In other words, with increasing RH the size of the first semicircle reduces quickly compared to that of the second one. As RH level reaches 53%, besides the two depressed semicircles in high frequency region, a nearly straight line emerges in low frequency region so that the complex impedance plots consist of three parts.

Such typical characteristics of the humidity sensor can be ascribed to a unique structure, consisting of nanorods, nanorod boundaries, and nanopores, and its schematic illustration is displayed in Fig. 10a and b. In terms of the complex impedance diagram shown in Figs. 8 and 9, their equivalent circuit can be built up, which contains a series array of parallel RC elements, as shown in Fig. 10c. R and C represent the resistance and the capacitance of the parallel circuit, respectively, i.e. the conduction and the polarization process, and R equals the magnitude of the diameter of the semicircle. In addition, it is known that at the peaks of the semicircles the equation $\omega\tau = 1$ holds well, where τ is the mean relaxation time and equals RC, and ω is the angular frequency at the maximum of the impedance imaginary component. Each individual component, i.e. the nanorod interior materials, the nanorod boundaries and pore-walls, and the electrode/nanorod film interfaces, is differentiated by its unique relaxation time (τ).

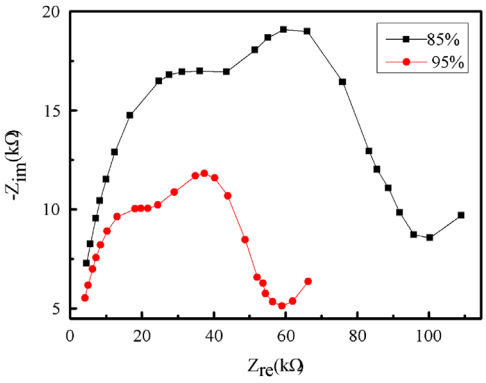

Fig. 9. Complex impedance plots of the humidity sensor based on the porous $ZnAl_2O_4$ nanorods measured in higher RH values of 85% and 95% within the frequency range from 40 Hz to 1 MHz.

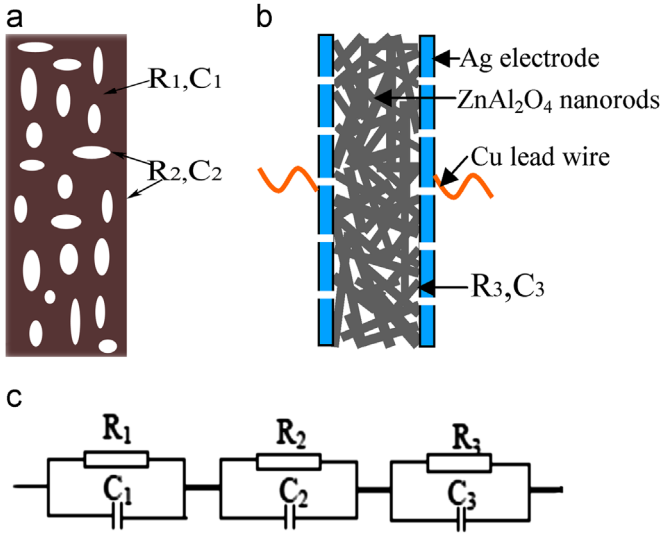

Fig. 10. (a) Sketch of a single porous $ZnAl_2O_4$ nanorod. (b) Schematic illustration of the humidity sensor based on porous $ZnAl_2O_4$ nanorods. (c) Equivalent circuit of the sensor. Parallel *RC* combinations with subscripts 1, 2, and 3 represent the nanorod interior materials, the nanorod boundaries and pore-walls, and the electrode/nanorod film interfaces, respectively.

At very low RH levels (below 11%), only a few water molecules are adsorbed, and furthermore, the coverage of water on nanorod boundaries and pore-walls is not continuous. Thus, the ionization rarely occurs and it is difficult for the electrolytic conduction. However, a high local charge density and a strong electrostatic field, presented in the tips and surface defects of nanorods, can promote water dissociation on the nanorod boundaries and pore-walls, and thus protons H^+ or H_3O^+, served as charge carriers of hopping transport, can be generated [34,35]. For $ZnAl_2O_4$ spinel, it is a well-known direct wide-bandgap semiconductor, whose optical bandgap has been estimated to be about 3.8 eV [36]; moreover large quantities of defects such as oxygen vacancies exist in the porous $ZnAl_2O_4$ nanostructures. Thus, charged carriers (conduction) and bounded electrons (polarization) can exist inside the semiconductor nanorods. In addition, the barrier formed on nanorod interface against the conduction of electron, which requires higher activation energies for hopping across them than the nanorods, and thus nanorod boundaries and pore-walls possess higher resistance than the nanorod interiors [37]. Although the protonic hopping transport between adjacent hydroxyl groups exists on the nanorod boundaries and pore-walls at very low RH, the resistance of nanorod interior materials is still lower than that of nanorod boundaries and pore-walls. Under 11% RH, therefore, the approximately single semicircle should mainly originate from the boundaries and pore-walls; however the size of the semicircle from the nanorod interior materials is relatively small and completely hidden inside the large semicircle.

As the RH increases from 33% to 85%, one or several water layers are formed on the immense nanorod boundaries and pore-walls, and thus physisorption begins to dominate. Moreover, the ionization and dissociation of water can be promoted hugely on the nanostructured surfaces. In addition, the motion of ions crossing the surface might be easier than the tightly packed grains. Therefore, the electrolytic conduction appears along with the protonic transport and becomes dominating in the transport-process. On the other hand, the charged ions may bend the energy-band of the surface of the sensing materials, and thus the electrical conductivity can also be enhanced by donating electrons to the conduction band of the base materials. As a consequence, the surface resistance can show a fast reduction compared to that of the interior materials, and correspondingly, the semicircle size exhibits a large decrease, and thus the semicircle from the nanorod interior materials can be observed noticeably and two major relaxation processes appear within the measurable frequency ranges. Because the nanorod boundaries possess higher resistance than nanorod interior materials at low RH levels [37], the semicircle in high frequency region should be from nanorod boundaries and pore-walls; while the semicircle in low frequency region is the result of the nanorod interior materials. Additionally, the moisture from the boundaries and pore-walls can diffuse into the interior structures, and hence the conductivity of nanorod interior materials can be enhanced and the corresponding semicircle size also decreases with increasing the RH from 33% to 85%. However, the amount of moisture content in the cell structures is negligible compared to the amount of moisture content on the nanorod boundaries and pore-walls at relatively low RH, and therefore the decrease of its size is relatively slow.

In higher RH ranges (above 85%), capillary condensation effects can take place, and moreover, Kelvin radius increases dramatically with RH [31]. Thus, more and more water vapor is condensed into the larger pores and the electrode/nanorod film interfaces. Since the pore-wall is very thin, meanwhile, the energy-band bend on the surface of the sensing materials is more serious and electrons transfer more easily to the conduction band, and moreover, the diffusion of

moisture into the cell structures cannot be ignored. Therefore, the resistances from the interior materials of nanorods also exhibit a considerable decease. As a result, the two semicircles with very close sizes superimpose in the complex impedance plot under 95% RH. In addition, because the water molecules adsorbed on the interfaces between the sensing film and the electrodes directly contact electrodes, more charged carriers are accumulated at the electrodes, and thus the orientation polarization occurs more readily. Therefore, the condensation of water vapor in the electrode/nanorod film interfaces not only makes the capacitance increase hugely, but also makes the charge transfer much faster than the diffusion of ionic species at the interfaces. As a consequence, a nearly straight line is observed in lower frequency region, which can be ascribed to the Warburg impedance [38]. Moreover, the higher the RH is, the longer the line is.

4. Conclusions

In summary, $ZnAl_2O_4$ nanorods, synthesized via a homogeneous co-precipitation method followed by a heat treatment at 900 °C, exhibit characteristics of porosity and a large specific surface area. As inspired by this, a humidity sensor based on the nanostructures was made. The adsorption sites of water vapor on nanorod boundaries and pore-walls can be increased efficiently; moreover a high local charge density and a strong electrostatic field, brought by the tips, oxygen vacancies, and surface defects, can also promote the dissociation of adsorbed water. Thus, a relatively high sensitivity can be achieved for the humidity sensor, such as the impedance changes from 7×10^3 to 70 kΩ as the RH varies from 11% to 98% at the measured frequency of 40 Hz. Meanwhile, good linearity, high reliability and stability, and small hysteresis can be obtained as well. Additionally, the porous nanostructures also provide an effective and fast channel for the transport of water vapor and liquid, and consequently, the sensor can show quick response and recovery time of about 15 and 30 s, respectively.

At very low RH (below about 11%), the resistance of the protonic hopping transport on nanorod boundaries and pore-walls is much higher than that of the electron transport inside $ZnAl_2O_4$ nanorods so that the complex impedance diagram looks like a single semicircle. With increasing RH, however, the fast decomposition of adsorbed water dominates gradually on nanorod boundaries and pore-walls. Thus, the electrolytic conduction along with protonic hopping transport takes place, resulting into a relative large decrease in surface resistance. As a consequence, the size of the corresponding semicircle shows a larger reduction than that of the semicircle from nanorod interior materials so that the latter can be observed clearly in low frequency region in the complex impedance plots. At RH above 85%, more and more water is condensed to larger nanopores and electrode/nanorod film interfaces due to a capillary condensation effect, and correspondingly, the sizes of the two semicircles both show larger decrease and a nearly straight line appears in lower frequency region. Our results indicate that porous $ZnAl_2O_4$ nanorods might be promising humidity sensing materials for practical application.

Acknowledgment

This work was supported by the Natural Science Foundation of China (51162023, and 21263013), and the Natural Science Foundation of Jiangxi Province (20114BAB206027). Y.H. Xiao and S.J. Lei thank for the support of the Natural Science Foundation of China (51002073, and 21001062).

References

[1] T.H. Huang, J.C. Chou, T.P. Sun, S.K. Hsiung, A device for skin moisture and environment humidity detection, Sensors and Actuators B 134 (2008) 206–212.
[2] Z. Chen, C. Lu, Humidity sensors: a review of materials and mechanisms, Sensor Letters 3 (2005) 274–295.
[3] S.J. Kim, J.Y. Park, S.H. Lee, S.H. Yi, Humidity sensors using porous silicon layer with mesa structure, Journal of Physics D 33 (2000) 1781–1784.
[4] S. Muto, O. Suzuki, T. Amano, M. Morisawa, A plastic optical fibre sensor for real-time humidity monitoring, Measurement Science and Technology 14 (2003) 746–750.
[5] P. Shuk, M. Greenblatt, Solid electrolyte film humidity sensor, Solid State Ionics 113 (1998) 229–233.
[6] M.V. Kulkarni, A.K. Viswanath, P.K. Khanna, Synthesis and humidity sensing properties of conducting poly (N-methyl aniline) doped with different acids, Sensors and Actuators B 115 (2006) 140–149.
[7] J. Shah, R.K. Kotnala, B. Singh, H. Kishan, Microstructure-dependent humidity sensitivity of porous $MgFe_2O_4$–CeO_2 ceramic, Sensors and Actuators B 128 (2007) 306–311.
[8] B.M. Kulwicki, Humidity sensors, Journal of the American Ceramic Society 74 (1991) 697–708.
[9] E. Traversa, Ceramic sensors for humidity detection: the state-of-the-art and future developments, Sensors and Actuators B 23 (1995) 135–156.
[10] P.M. Faia, C.S. Furtado, A.J. Ferreira, Humidity sensing properties of a thick-film titania prepared by a slow spinning process, Sensors and Actuators B 101 (2004) 183–190.
[11] Y. Zhang, K. Yu, S. Ouyang, L. Luo, H. Hu, Q. Zhang, Z. Zhu, Detection of humidity based on quartz crystal microbalance coated with ZnO nanostructure films, Physica B 368 (2005) 94–99.
[12] G. Sberveglieri, G. Rinchetti, S. Groppelli, G. Faglia, Capacitive humidity sensor with controlled performances, based on porous Al_2O_3 thin film growm on SiO_2–Si substrate, Sensors and Actuators B 19 (1994) 551–553.
[13] B.C. Cheng, B.X. Tian, C.C. Xie, Y.H. Xiao, S.J. Lei, Highly sensitive humidity sensor based on amorphous Al_2O_3 nanotubes, Journal of Materials Chemistry 21 (2011) 1907–1912.
[14] S. Agarwal, G.L. Sharma, Humidity sensing properties of (Ba,Sr)-TiO_3 thin films grown by hydrothermal–electrochemical method, Sensors and Actuators B 85 (2002) 205–211.
[15] J. Yuk, T. Troczynski, Sol–gel $BaTiO_3$ thin film for humidity sensors, Sensors and Actuators B 94 (2003) 290–293.
[16] J. Kong, N.R. Franklin, C. Zhou, M.G. Chapline, S. Peng, K. Cho, H. Dai, Nanotube molecular wires as chemical sensors, Science 287 (2000) 622–625.
[17] Q. Wan, Q.H. Li, Y.J. Chen, T.H. Wang, X.L. He, X.G. Gao, J.P. Li, Positive temperature coefficient resistance and humidity

sensing properties of Cd-doped ZnO nanowires, Applied Physics Letters 84 (2004) 3085–3087.
[18] H. Jamil, S.S. Batool, Z. Imran, M. Usman, M.A.M. Rafiq, M.M. Hassan, Lectrospun titanium dioxide nanofiber humidity sensors with high sensitivity, Ceramics International 38 (2012) 2437–2441.
[19] D. Zhang, Z. Liu, C. Li, T. Tang, X. Liu, S. Han, B. Lei, C. Zhou, Detection of NO_2 down to ppb levels using individual and multiple In_2O_3 nanowire devices, Nano Letters 4 (2004) 1919–1924.
[20] Z. Zhang, C.G. Hu, Y.F. Xiong, R. Yang, Z.L. Wang, Synthesis of Ba-doped CeO_2 nanowires and their application as humidity sensors, Nanotechnology 18 (2007) 465504.
[21] G.Q. Wu, J.W. Zhang, X.Y. Wang, J.J. Liao, H. Xia, S.A. Akbar, J.B. Li, S.W. Lin, X.G. Li, J. Wang, Hierarchical structured TiO_2 nano-tubes for formaldehyde sensing, Ceramics International 38 (2012) 6341–6347.
[22] B.C. Cheng, S.C. Qu, H.Y. Zhou, Z.G. Wang, Porous $ZnAl_2O_4$ spinel nanorods doped with Eu^{3+}: synthesis and photoluminescence, Nanotechnology 17 (2006) 2982.
[23] M. Tahhan, V. Truong, G. Spinks, G. Wallace, Carbon nanotube and polyaniline composite actuators, Smart Materials and Structures 12 (2003) 626–632.
[24] O. Varghese, D. Gong, M. Paulose, K. Ong, C. Grimes, E. Dickey, Highly ordered nanoporous alumina films: effect of pore size and uniformity on sensing performance, Journal of Materials Research 17 (2002) 1162–1171.
[25] J.J. Vijaya, L.J. Kennedy, A. Meenakshisundaram, G. Sekaran, K.S. Nagaraja, Humidity sensing characteristics of sol-gel derived Sr(II)-added $ZnAl_2O_4$ composites, Sensors and Actuators B 127 (2007) 619–624.
[26] J. Wang, F. Wu, K. Shi, X. Wang, P. Sun, Humidity sensitivity of composite material of lanthanum ferrite/polymer quaternary acrylic resin, Sensors and Actuators B 99 (2004) 586–591.
[27] B.C. Cheng, S.C. Qu, H.Y. Zhou, Z.G. Wang, Al_2O_3: Cr^{3+} nanotubes synthesized via homogenization precipitation followed by heat treatment, Journal of Physical Chemistry B 110 (2006) 15749–15754.
[28] V. Bondarenka, S. Grebinskij, S. Mickeviius, V. Volkov, G. Zacharova, Thin films of poly-vanadium–molybdenum acid as starting materials for humidity sensors, Sensors and Actuators B 28 (1995) 227–231.
[29] J. Wang, H. Wan, Q. Lin, Properties of a nanocrystalline barium titanate on silicon humidity sensor, Measurement Science and Technology 14 (2003) 172–175.
[30] T. Seiyama, N. Yamazoe, H. Arai, Ceramic humidity sensors, Sensors and Actuators 4 (1983) 85–96.
[31] W. Chen, Z. Zhao, X. Liu, Z. Zhang, C. Suo, A capacitive humidity sensor based on multi-wall carbon nanotubes (MWCNTs), Sensors 9 (2009) 7431–7444.
[32] S. Gregg, The Surface Chemistry of Solids, Chapman & Hall, London, 1961.
[33] V. Timár-Horváth, L. Juhász, A. Vass-Várnai, G. Perlaky, Usage of porous Al_2O_3 layers for RH sensing, Microsystem Technologies 14 (2008) 1081–1086.
[34] R. Schaub, P. Thostrup, N. Lopez, E. Laegsgaard, I. Stensgaard, J.N. rskov, F. Besenbacher, Oxygen vacancies as active sites for water dissociation on rutile TiO_2(110), Physical Review Letters 87 (2001) 266104.
[35] N. Yamazoe, Y. Shimizu, Humidity sensors: principles and applications, Sensors and Actuators 10 (1986) 379–398.
[36] S. Sampath, J. Cordaro, Optical properties of zinc aluminate, zinc gallate, and zinc aluminogallate spinels, Journal of the American Ceramic Society 81 (1998) 649–654.
[37] P. Victor, S. Bhattacharyya, S. Krupanidhi, Dielectric relaxation in laser ablated polycrystalline ZrTiO thin films, Journal of Applied Physics 94 (2003) 5135–5142.
[38] P. Christensen, A. Hamnett, Techniques and Mechanisms in Electrochemistry, Springer, Netherlands, 1994.